# ARTICLE

Check for updates

Bulk tungsten-substituted vanadium oxide for low-temperature NOx removal in the presence of water

Yusuke Inomata [1], Hiroe Kubota[2], Shinichi Hata[3], Eiji Kiyonaga[4], Keiichiro Morita[4], Kazuhiro Yoshida[4], Norihito Sakaguchi [5], Takashi Toyao [2], Ken-ichi Shimizu[2,8], Satoshi Ishikawa[6], Wataru Ueda[6], Masatake Haruta[1] & Toru Murayama [1,7,8]✉

NH$_3$-SCR (selective catalytic reduction) is important process for removal of NOx. However, water vapor included in exhaust gases critically inhibits the reaction in a low temperature range. Here, we report bulk W-substituted vanadium oxide catalysts for NH$_3$-SCR at a low temperature (100–150 °C) and in the presence of water (~20 vol%). The 3.5 mol% W-substituted vanadium oxide shows >99% (dry) and ~93% (wet, 5–20 vol% water) NO conversion at 150 °C (250 ppm NO, 250 ppm NH$_3$, 4% O$_2$, SV = 40000 mL h^{-1} g$_{cat}$$^{-1}$). Lewis acid sites of W-substituted vanadium oxide are converted to Brønsted acid sites under a wet condition while the distribution of Brønsted and Lewis acid sites does not change without tungsten. NH$_4$$^+$ species adsorbed on Brønsted acid sites react with NO accompanied by the reduction of V^{5+} sites at 150 °C. The high redox ability and reactivity of Brønsted acid sites are observed for bulk W-substituted vanadium oxide at a low temperature in the presence of water, and thus the catalytic cycle is less affected by water vapor.

[1] Research Center for Gold Chemistry, Graduate School of Urban Environmental Sciences, Tokyo Metropolitan University Hachioji, Tokyo 192-0397, Japan. [2] Institute for Catalysis, Hokkaido University, Sapporo, Hokkaido 001-0021, Japan. [3] Department of Applied Chemistry, Faculty of Engineering, Sanyo-Onoda City University, Sanyo-Onoda, Yamaguchi 756-0884, Japan. [4] Energia Economic and Technical Research Institute, The Chugoku Electric Power Company, Incorporated, Higashihiroshima, Hiroshima 739-0046, Japan. [5] Laboratory of Integrated Function Materials, Center for Advanced Research of Energy and Materials, Faculty of Engineering, Hokkaido University, Sapporo, Hokkaido 060-8628, Japan. [6] Department of Material and Life Chemistry, Faculty of Engineering, Kanagawa University, Yokohama, Kanagawa 221-8686, Japan. [7] Yantai Key Laboratory of Gold Catalysis and Engineering, Shandong Applied Research Center of Gold Nanotechnology (Au-SDARC) School of Chemistry and Chemical Engineering, Yantai University, Yantai 264005, China. [8] These authors jointly supervised this work: Ken-ichi Shimizu, Toru Murayama. ✉email: murayama@tmu.ac.jp

1

Emission control of NO_x (NO and NO_2) is an important task for an industrial chemical process that relies on thermal energy produced by the combustion of fossil fuels. For stationary $deNO_x$ systems such as those in coal-fired power plants and waste treatment plants, selective catalytic reduction (SCR) has been used with ammonia as a reducing reagent to convert harmful NO_x to harmless N_2 and H_2O[1–3]:

$$4NO + 4NH_3 + O_2 \rightarrow 4N_2 + 6H_2O. \qquad (1)$$
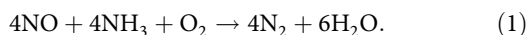
Although the stationary $deNO_x$ systems have been successfully established, a conventional catalyst needs a high temperature (>300 °C) for NH_3-SCR to proceed[3,4]. In most cases, $deNO_x$ catalysts are placed just after the boiler system for a high reaction temperature[4]. Consequently, $deNO_x$ catalysts are deactivated by ash and sulfate generated from the reaction of ammonia and SO_2 because the catalysts are exposed to the gas before passing through the dust collection and $deSO_x$ system. $DeNO_x$ catalysts can be moved to the latter part of the system to avoid the deactivation of the $deNO_x$ catalyst works at a low temperature (<150 °C) since the downstream gas is usually cooled down to 100–150 °C.

Vanadium (V) oxide-based catalysts (V_2O_5/TiO_2, V_2O_5–WO_3/TiO_2) have been used as industrial catalysts for stationary boiler systems because they show high N_2 selectivity, good thermal stability, and low SO_2 oxidation activity to SO_3[2]. However, their high working temperature limits the latitude of the $deNO_x$ process. Therefore, many studies have been carried out to develop low-temperature SCR catalysts such as metal oxide-based materials (V, Mn, Cr, Cu, W, Ce, and Fe)[1,5–10] and ion-exchanged zeolite (Cu-ZSM-5, Fe-ZSM-5, Cu-CHA, and Cu-SSZ-13)[1,11–17].

We previously showed that vanadium oxide with a bulk crystal structure works as an NH_3-SCR catalyst at a low temperature (<150 °C) with high N_2 selectivity and less SO_2 oxidation activity in contrast to the supported vanadia species[18,19]. Recent studies provided an insight into the effect of the coordination environment, atomic configuration, and vanadium surface density of the catalyst on SCR activity[20–22]. It was proposed in previous reports that supported vanadia catalysts are composed of VO_4 units with O-exposed moieties[2,23]. On the other hand, bulk V_2O_5 has a metal (V)-exposed part in addition to the O-exposed part[24], and it might show a different catalytic property from that of a supported vanadia catalyst because of their different redox properties, bond strengths, and coordination environments[23,25]. Bulk crystal of V_2O_5 is composed of a two-dimensional sheet structure with VO_5 units that are connected by a weak van der Waals force[24,26–29]. Consequently, the morphology of V_2O_5 is thermally reconstructed because of its weak interaction in the crystal structure. According to previous studies, the poor stability of V_2O_5 can be overcome by doping another metal with a three-dimensional coordination environment[30–32]. Bulk tungsten oxide (WO_3) is composed of WO_6 units that are three-dimensionally connected[33–35]. Furthermore, WO_3 is known as a promoter for supported vanadia catalysts that enhance the reactivity of vanadia sites[36]. Therefore, the incorporation of tungsten sites into bulk V_2O_5 would facilitate not only the NH_3-SCR activity but also the structural stability of bulk vanadium oxide-based catalysts.

The negative effect of water, which is intrinsically included in the exhaust gas (10–30 vol%)[2], is critical for low-temperature NH_3-SCR, while the effect would be much less in a high-temperature range. The effect of water is thought to be inhibition of the adsorption of the reactant[37–43] and/or the reaction between NO and adsorbed NH_3[44–46]. The water adsorption behavior was studied for a V_2O_5–WO_3 solid solution system and V_2O_5 without tungsten[47–49]. Broclawik et al.[48] theoretically suggested that dissociative adsorption of water occurs on adjacent V–O–W sites, leading to an increase in the concentration of Brønsted acid sites.

On the other hand, water merely adsorbs in the case of V_2O_5 without tungsten, and a Brønsted acid site is not newly created. Thus, NH_3-SCR would efficiently proceed with a vanadium–tungsten complex oxide even in the presence of water vapor owing to the large population of protonic Brønsted acid sites.

The reaction mechanisms of NH_3-SCR have been widely investigated for a supported vanadium-based oxide catalyst under a dry gas condition using in situ and operando spectroscopic techniques (infrared (IR), ultraviolet–visible (UV–Vis), Raman)[20,36,38,46,50–54]. The current consensus is that both Lewis acid and Brønsted acid sites participate in the reaction mechanism. The reaction mechanism should be investigated in the presence of water as well as under dry conditions in order to understand catalytic activity in the actual atmosphere. Although Topsøe et al.[45] and Song et al.[55] investigated the reaction mechanism of 3–6 wt% V_2O_5/TiO_2 under a 1.7–3.0 vol% water atmosphere at 250–300 °C, the reaction mechanism of the vanadium–WO_3 system has not been investigated under wet conditions, especially in a low-temperature range. An insight into the reaction mechanism under wet conditions would provide a milestone for designing the active site of a low-temperature NH_3-SCR catalyst under actual conditions.

Herein, we report a bulk tungsten-substituted vanadium oxide catalyst for low-temperature NH_3-SCR (<150 °C) under a wet atmosphere. The structural features of bulk tungsten-substituted vanadium oxide are studied. We examine the effect of tungsten substitution on water tolerance to NH_3-SCR activity and catalytic stability. The reaction mechanism is investigated by operando spectroscopies under dry and wet conditions to elucidate the role of vanadium and tungsten sites in the catalytic cycle. Finally, we compare the difference between bulk tungsten-substituted vanadium oxide catalyst and a current titania-supported vanadia catalyst.

Results

Synthesis of tungsten-substituted vanadium oxide. Tungsten-substituted vanadium oxide was synthesized by the oxalate method using ammonia metavanadate, ammonia metatungstate, and oxalic acid. Water-insoluble ammonia metavanadate was converted to soluble vanadium oxalate in aqueous media, and ammonia metatungstate was then added to the aqueous solution followed by evaporation. The resulting precursor powder was then calcined in air. The synthesized x mol% tungsten-substituted vanadium oxides were denoted as xW–V (x = 0, 1, 3.5, 7, 10, 15, and 40). The precursor powder of the 3.5W–V sample showed a strong exothermic peak assigned to its decomposition at around 297 °C from thermogravimetry/differential thermal analysis measurement (Supplementary Fig. 2). Thus, we calcined the catalyst twice at 300 °C for 4 h each time to obtain V_2O_5-based catalysts with large surface areas. The specific surface areas of the xW–V (x = 0–40) catalysts were measured to be 32–41 $m^2 g^{-1}$ (Supplementary Table 2), which are almost in the same range and comparably large.

**Characterization of tungsten-substituted vanadium oxide**. Atomic-resolution high-angle annular dark-field imaging-scanning transmission electron microscopy (HAADF-STEM) images were measured to directly determine the incorporation of tungsten into vanadium oxide. The image of 0W–V (V_2O_5 without tungsten) showed a lattice fringe based on the (101) plane (Fig. 1a). No bright spots of tungsten atoms were observed for 0W–V. On the other hand, we confirmed atomic bright spots on the vanadium oxide lattice for 3.5W–V (Fig. 1b), indicating that tungsten atoms were atomically dispersed. An enlarged view of
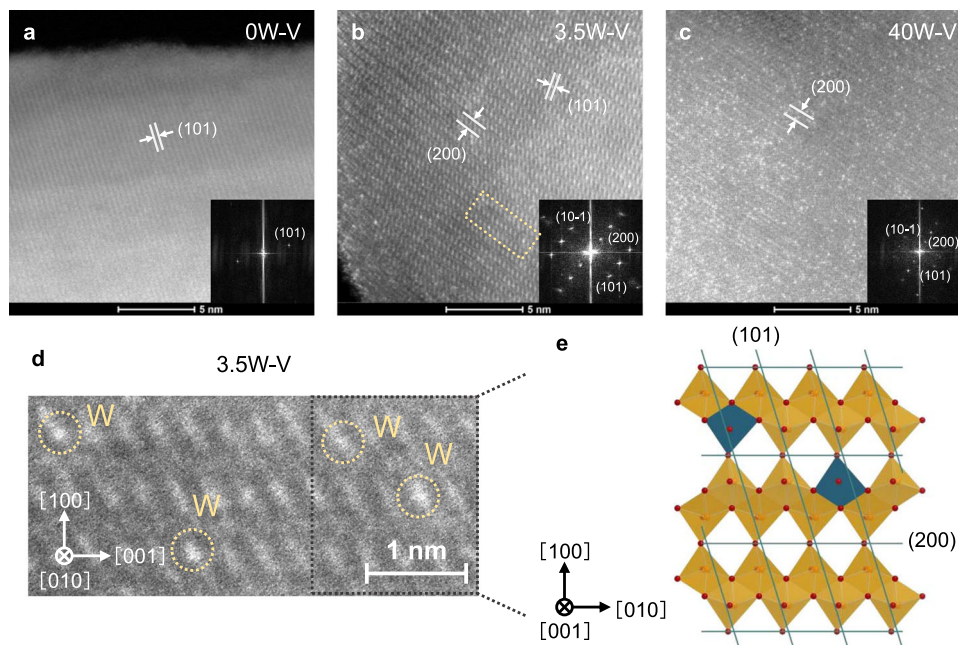
Fig. 1 Direct observation of tungsten substitution. HAADF-STEM images of **a** 0, **b** 3.5, and **c** 40 mol% W-substituted vanadium oxide (0, 3.5, and 40W–V). Insets: corresponding FFT images. **d** Enlarged view of the yellow region in (**b**). **e** Crystal structure of W-substituted vanadium oxide. Orange polyhedra: vanadium units; blue polyhedra: tungsten units.

the HAADF-STEM image for 3.5W–V (Fig. 1d) showed that lattice vanadium atoms were partially substituted by tungsten atoms (Fig. 1e). Aggregated tungsten sites were observed on the surfaces of catalysts when 7 mol% tungsten was added to vanadium oxide (7W–V; Supplementary Fig. 3). Adjacent and aggregated tungsten moieties were more clearly observed when 40 mol% tungsten was added to vanadium oxide (40W–V; Fig. 1c), indicating that a WO_3 phase partially forms with an increase in the amount of tungsten. Thus, 0, 3.5, and 40W–V can be regarded as catalysts without tungsten, with a moderate amount of tungsten and with an excess amount of tungsten, respectively.

The crystal structures of xW–V were confirmed from X-ray powder diffraction (XRD) measurements to determine the effect of tungsten doping (Fig. 2a). For 0, 1, and 3.5W–V, all of the diffraction peaks were assigned as vanadium oxide phase (Fig. 2a, b), and no WO_3 crystalline phase was confirmed. Given that the HAADF-STEM images showed tungsten dispersed atomically, the XRD patterns suggested that tungsten atoms were atomically incorporated into the vanadium oxide lattice and a W–V oxide solid solution was formed. We confirmed broad XRD peaks of WO_3 (Fig. 2a, c) at $2\theta = 23°$ for 7, 10, 15, and 40W–V in addition to the XRD patterns of vanadium oxide. These results indicate that tiny WO_3 crystalline particles form when the tungsten content is higher than 7 mol% as shown by HAADF-STEM images. The peak positions of (010) reflection at around $2\theta = 20.2°$ slightly increased with an increase in the amount of tungsten (Fig. 2a, inset), indicating that the lattice spacing decreased along the b-axis. The lattice parameters were calculated by Rietveld analysis. The lattice parameters of the b-axis decreased with an increase in the amount of tungsten (Supplementary Fig. 4b). These results show that WO_6 units connect the vanadium oxide layers by bond formation (e.g., V= O → V–O–W). The lattice parameters along the a-axis and c-axis were expanded because of the incorporation of tungsten atoms with a larger ionic radius (Supplementary Fig. 4a, c).
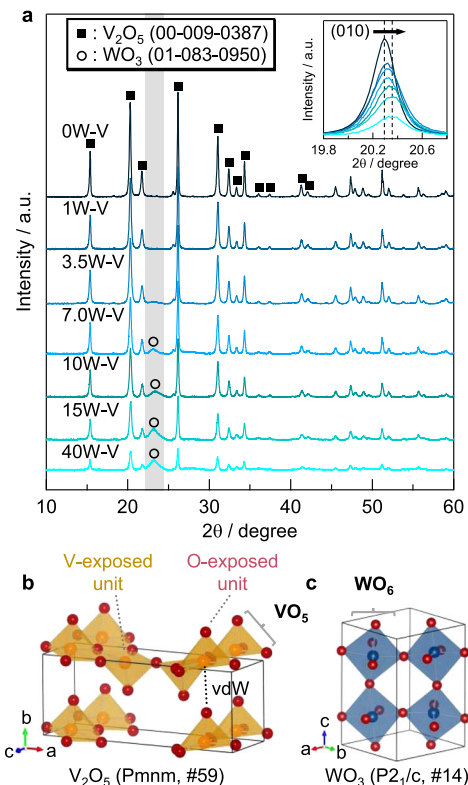
Fig. 2 Crystal structures of W-substituted vanadium oxide catalysts. a XRD patterns of W-substituted vanadium oxide catalysts. Inset: enlarged view of peaks corresponding to (010) reflection. (All of the peaks $2\theta > 40°$ were also assigned to V_2O_5.) Crystal structures of **b** V_2O_5 and **c** WO_3. Orange polyhedra: VO_5 units; blue polyhedra: WO_6 units. VdW van der Waals force.

We also conducted IR measurements for 0, 3.5, and 40W–V to determine the effect of tungsten substitution on the structure (Supplementary Fig. 5). Although an obvious difference in the infrared (IR) spectra was not found for 3.5 and 0W–V, the IR peak of 40W–V assigned to V = O (1020 cm^{-1}) became weak compared to those of 0 and 3.5W–V, results similar to those reported by Satsuma et al.[56]. The number of V = O bonds would decrease to form V–O–W bonds by the addition of tungsten into the vanadium oxide lattice.

NH₃-SCR activity of tungsten-substituted vanadium oxide. First, we investigated the effects of different amounts of tungsten on the NH₃-SCR activity of xW–V catalysts under dry and wet (10 vol% water) atmospheres at 150 °C (Fig. 3a). The 0W–V catalyst (V₂O₅ without tungsten) showed NO conversions of 82% (dry) and 47% (wet). The NO conversion increased with an increase in the amount of tungsten up to 3.5 mol%. The NO conversions of 3.5W–V were >99% (dry) and 94% (wet). The negative effect of water was suppressed by the incorporation of tungsten into vanadium oxide. The 3.5W–V catalyst showed the best NH₃-SCR activity among the synthesized catalysts, while the NO conversion decreased with a further increase in the amount of tungsten. The 40W–V catalyst showed NO conversions of 29% (dry) and 19% (wet). Thus, an excess amount of tungsten decreased the NH₃-SCR activity.

The dependence of NO conversion on reaction temperature was examined for 0W–V, 3.5W–V, and 1 wt% V₂O₅–5 wt% WO₃/TiO₂ (V–W/TiO₂, a model of an industrial catalyst; Fig. 3b). The 3.5W–V catalyst showed NH₃-SCR activity at a low temperature (<150 °C) under both dry and wet conditions in which the conventional

V–W/TiO₂ catalyst did not show sufficient NH₃-SCR activity. The 0W–V catalyst (V₂O₅ without tungsten) also showed low-temperature NH₃-SCR activity under a dry condition, but the negative effect of water was critical at a low temperature. The temperatures for 80% NO conversion (T_{80}) were 110 °C (3.5W–V), 157 °C (0W–V), and 225 °C (V–W/TiO₂) under a dry condition and 135 °C (3.5W–V), 178 °C (0W–V), and 236 °C (V–W/TiO₂) under a wet (10 vol% water) condition. N₂ selectivity was >99% during the reaction, and undesirable N₂O production was not observed for any of the catalysts (Supplementary Fig. 6).
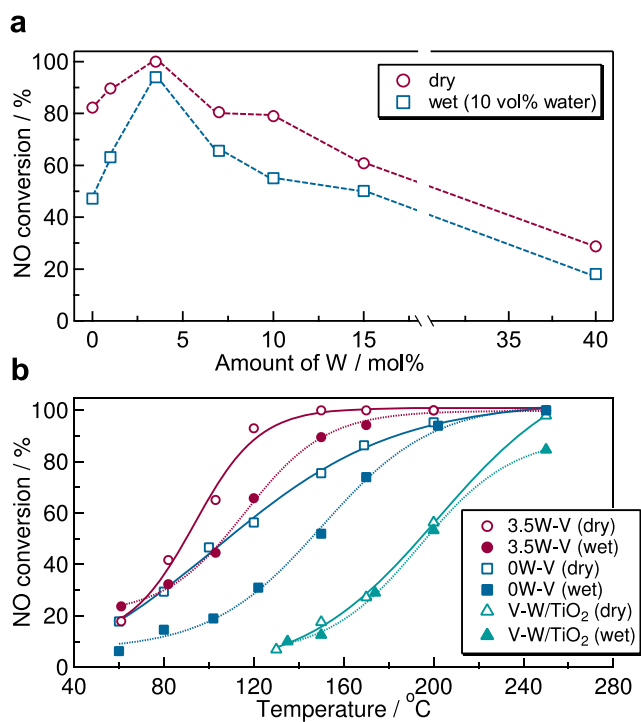
The effects of water concentration in flow gas on NH₃-SCR were also investigated for 0W–V and 3.5W–V at 150 °C (Fig. 4a). Although NO conversion of 3.5W–V was slightly decreased by the addition of 5% water into reaction gas, ~93% NO conversion was maintained in the presence of 5–20 vol% of water. On the other hand, NO conversion was drastically decreased from 82% to 35% in the case of 0W–V when water vapor was introduced to the reaction gas. Although NO conversion decreased with the addition of water, the values were almost the same regardless of the concentration of water (2–20%). Previous studies showed that a further inhibitory effect of water on the reaction rate did not occur at a high water concentration (>5%)[2,39,57]. Water vapor would affect a catalytic cycle more strongly at a low temperature such as 150 °C. Thus, we found that tungsten-doped vanadium oxide (3.5W–V) shows a low-temperature NH₃-SCR activity in the presence of a high concentration of water.

A catalytic stability test (150 °C) was conducted for 0W–V and 3.5W–V to determine the effect of tungsten on the stability (Fig. 4b). In the presence of 10 vol% water, the NO conversion was decreased for both 0W–V and 3.5W–V. After turning off the water addition, the NO conversion of 3.5W–V recovered to the original value (>99%), but that of 0W–V decreased from 78 to 59%. The specific surface areas of 0 and 3.5W–V were measured before and after the catalytic stability test (Fig. 4c). The specific surface area of 0W–V decreased after the stability test (41 → 19 m² g⁻¹), while 3.5W–V had the same value (39 m² g⁻¹). Although a porous structure was confirmed by scanning electron microscope measurement for 0W–V before the activity test, it disappeared and the surface became smooth after the test (Supplementary Fig. 7). Obvious morphological changes were not confirmed for 3.5W–V. There were no changes in the XRD patterns of 0 and 3.5W–V after the stability test (Supplementary Fig. 8). We assume that the bulk tungsten sites, which have a three-dimensional coordination environment (WO₆ units), retain the structure by incorporation into the layered vanadium oxide lattice, leading to the retention of surface area.
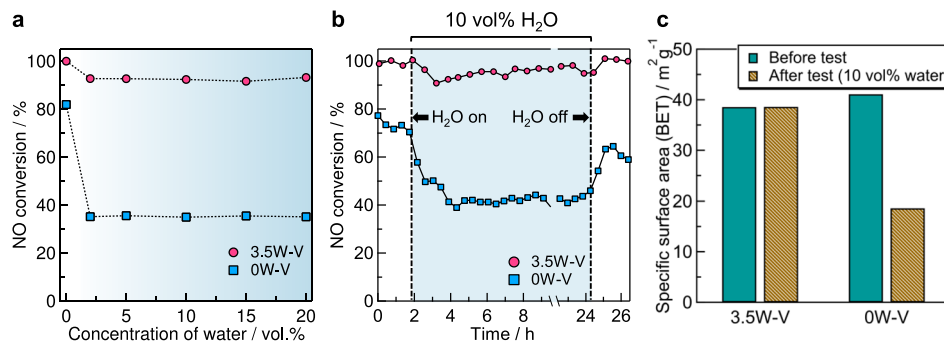

Fig. 3 NH₃-SCR activity of W-substituted vanadium oxide catalysts. a NO conversion (150 °C) of W-substituted vanadium oxide catalysts as a function of the molar ratio of tungsten. **b** NO conversion of 3.5W–V (W-substituted vanadium oxide), 0W–V (without tungsten), and V–W/TiO₂ (model of a conventional catalyst) as a function of reaction temperature. Reaction conditions: the amount of the catalyst, 0.375 g; reaction gas mixture, 250 ppm NO, 250 ppm NH₃, 4 vol% O₂ and 10 vol% H₂O (when used) in Ar; flow rate, 250 mL min⁻¹; space velocity, 40,000 mL h⁻¹ g$_{cat}$⁻¹.

Reaction kinetics of tungsten-substituted vanadium oxide catalysts. Reaction rate, apparent activation energy (E_a), and reaction order were investigated to understand the reaction kinetics for low-temperature NH₃-SCR. Reaction rates for the kinetics were calculated by adjusting the weights of the catalysts to control the conversion to <20%. Reaction rates per surface area were 3.2 × 10⁻⁹ (0W–V), 5.2 × 10⁻⁹ (3.5W–V), and 0.2 × 10⁻⁹ mol$_{NO}$ m⁻² s⁻¹ (V–W/TiO₂) in a dry condition (Fig. 5a and Supplementary Table 3), indicating that the reaction site of 3.5W–V was favorable for NH₃-SCR to proceed compared to the reaction sites of 0W–V and V–W/TiO₂. The reaction rate of 0W–V considerably decreased to 1.4 × 10⁻⁹ mol$_{NO}$ m⁻² s⁻¹ in a wet condition and that of 3.5W–V was 4.2 × 10⁻⁹ mol$_{NO}$ m⁻² s⁻¹. Thus, the inhibitory effect of water on the reaction was less for the tungsten-substituted vanadium oxide catalyst.
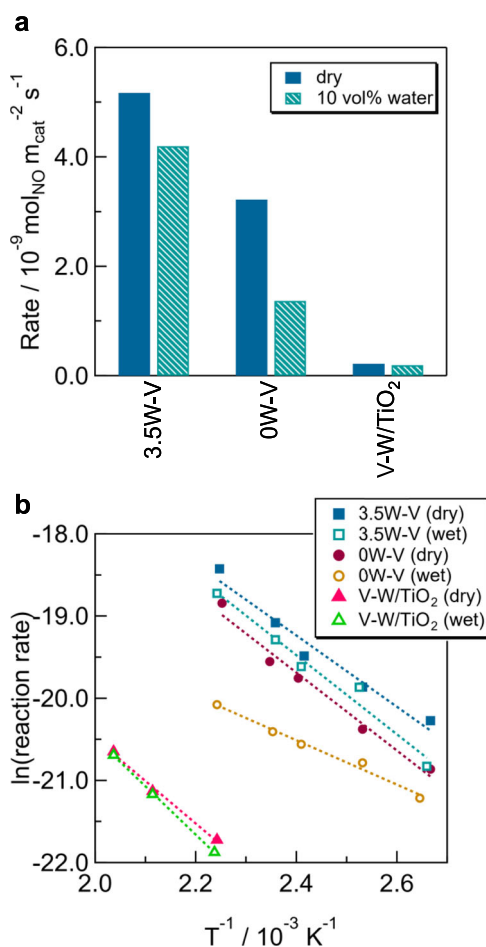
The apparent activation energy (E_a) values calculated from Arrhenius plots were 39 kJ mol⁻¹ (0W–V) and 36 kJ mol⁻¹ (3.5W–V) under a dry condition (Fig. 5b and Supplementary

Fig. 4 Water tolerance of W-substituted vanadium oxide catalysts. a NO conversion (150 °C) of 3.5W–V (W-substituted vanadium oxide) and 0W–V (without tungsten) as a function of the concentration of water. **b** Catalytic stability test (150 °C) of 3.5W–V and 0W–V. Reaction conditions: the amount of the catalyst, 0.375 g; reaction gas mixture, 250 ppm NO, 250 ppm NH₃, 4 vol% O₂ and 2–20 vol% H₂O (when used) in Ar; flow rate, 250 mL min⁻¹; space velocity, 40,000 mL h⁻¹ g$_{cat}$⁻¹. **c** Specific surface areas of 3.5W–V and 0W–V before and after a stability test.
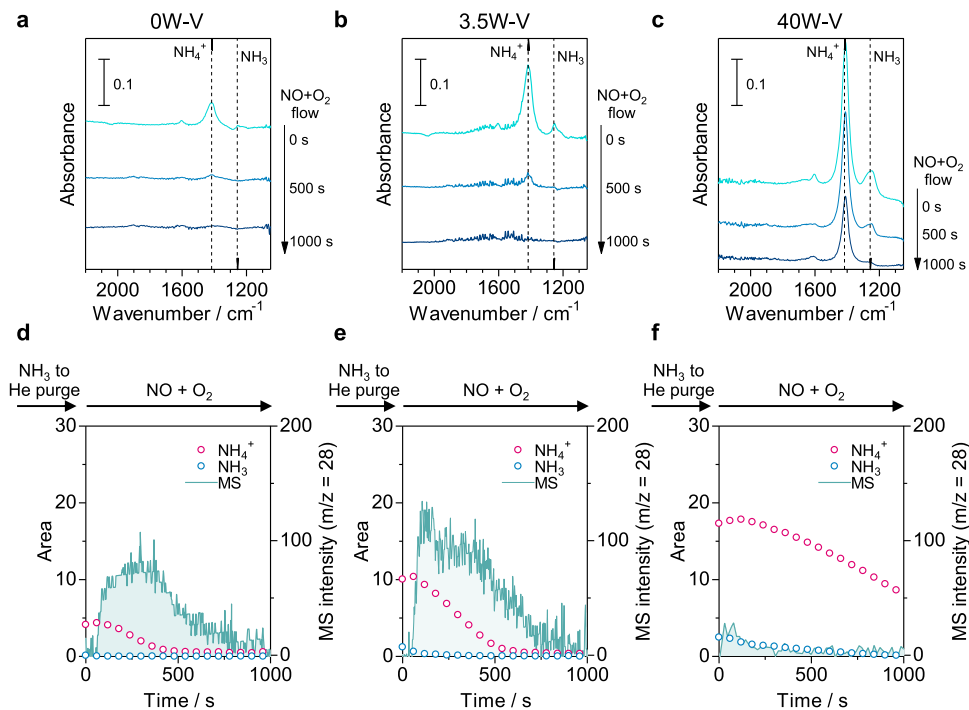

Fig. 5 Kinetic measurements for NH₃-SCR. a Reaction rate per specific surface area at 150 °C and **b** Arrhenius plots for 3.5W–V (W-substituted vanadium oxide), 0W–V (without tungsten), and V-W/TiO₂ (model of a conventional catalyst) at 150 °C under a dry condition and wet condition (10 vol% water).

(preexponential factor) would decrease because of its blockage by water, leading to a decrease in the activity. E_a values of V–W/TiO₂ were 43 (dry) and 49 kJ mol⁻¹ (wet). Therefore, the effect of tungsten on the NH₃-SCR cycle would be similar to that in the bulk V–W oxide system.

The NH₃-SCR of a vanadium-based catalyst proceeds as follows: (1) adsorption of NH₃ on an acid site, (2) reaction of NO with NH₃ to produce N₂ + H₂O via a nitrosamide (NH₂NO*) intermediate with simultaneous reduction of the vanadia surface, and (3) re-oxidation of the partially reduced vanadia surface by oxygen molecules[1,52,53]. Therefore, we measured the reaction orders for NH₃, NO, and O₂ at 150 °C (Supplementary Fig. 9 and Supplementary Table 3). Ranges of gas concentration were 125–500 ppm for NH₃, 125–500 ppm for NO, and 2–8% for O₂. Reaction orders of 0W–V and 3.5W–V were 0.2–0.3 (NH₃), 0.9–1.1 (NO), and 0.3–0.4 (O₂) under both dry and wet atmospheres. The small reaction order for NH₃ indicates that the adsorption of NH₃ to the catalyst surface is strong. The reaction order for NO was high compared to those for the other substrates, indicating that the reaction rate depended on NO concentration in actual conditions. The reaction order for O₂ was 0.3–0.4 at 150 °C, although zero-order dependence was reported at O₂ concentrations >1% at a higher temperature (>250 °C) for a supported vanadia catalyst[2,38,53]. Oxygen molecules contribute to the re-oxidation step of the partially reduced vanadia surface (V⁴⁺ → V⁵⁺) in the reaction mechanism of NH₃-SCR. However, the re-oxidation rate can be slower for a low temperature and the surface of the catalyst is not fully oxidized in a low-temperature range[2,38,53,54].

Roles of tungsten substitution in the NH₃-SCR cycle. We carried out *operando* IR and UV–Vis measurements at 150 °C to examine the reaction mechanism of NH₃-SCR over tungsten-substituted vanadium oxide catalysts at a low temperature. To observe the behavior of acid sites, we conducted *operando* IR measurements for 0W–V (V₂O₅ without tungsten), 3.5W–V (the most active catalyst), and 40W–V (with excess tungsten) as shown in Fig. 6. We flowed 0.1% NH₃/He to the IR discs of the catalysts to adsorb ammonia and purged excess ammonia with He. Then, the time course of the IR spectra was monitored under the condition of 500 ppm NO + 8% O₂/He flow with simultaneous detection of N₂ by a mass spectrometer (MS) equipped at the outlet of the IR cell. During this measurement, adsorbed NH₃ reacts with NO followed by reduction of redox-active sites. Then, reduced sites are re-oxidized by oxygen. The reaction would continue until adsorbed NH₃ is completely consumed (Supplementary Fig. 10). The amount of ammonia species adsorbed on Lewis and Brønsted acid sites was calculated from the area of corresponding IR peaks. Under the dry condition, IR peaks

Table 3), indicating that the reaction mechanisms were similar under a dry condition. E_a of 3.5W–V under a wet condition was 40 kJ mol⁻¹, which was close to that under a dry condition, but that of 0W–V was 22 kJ mol⁻¹ and preexponential factor (intercept of the line) decreased in the presence of water vapor. The change in E_a of 0W–V reflects the different reaction mechanism of vanadium oxide without tungsten. Although the E_a of 0W–V became smaller, the number of active sites

Fig. 6 Acid properties under a dry atmosphere. a–c *Operando* IR spectra of ad species on 0W–V (without tungsten), 3.5W–V (with tungsten), and 40W–V (excess tungsten) during NH_3 adsorption followed by $NO + O_2$ exposure at 150 °C under a dry condition. The IR disc was exposed to 0.1% NH_3/He flow (30 min) and purged with He (20 min), followed by exposure to 500 ppm $NO + 8\%$ O_2 (He balance) flow. **d–f** IR peak areas of ammonia species adsorbed on Lewis acid sites (NH_3) and Brønsted acid sites (NH_4^+) and MS intensity of N_2 versus time of $NO + O_2$ flowing.

assigned to NH_3 adsorbed on the Lewis acid site (1250–1254 cm^{-1}) and NH_4^+ adsorbed on Brønsted acid site (1410–1420 cm^{-1}) were observed for 0, 3.5, and 40W–V after the adsorption of ammonia (Fig. 6a–c). The relative amounts of Lewis and Brønsted acid sites, which were calculated from the area of initial IR peaks after ammonia adsorption (spectra at 0 s in Fig. 6a–c), were summarized in Fig. 7a. The numbers of acid sites increased from 0.1 to 2.5 (Lewis acid, NH_3) and from 4.1 to 17.3 (Brønsted acid, NH_4^+) with an increase in the molar ratio of tungsten in the catalysts up to 40 mol%. The results indicate that both Lewis and Brønsted acid sites are created by the incorporation of tungsten. The areas of the IR peaks for NH_3 and NH_4^+ decreased with time of $NO + O_2$ flow for 1000 s (Fig. 6a–c and d–f, red and blue lines). The consumption of ammonia species was completed within 500 s for 0 and 3.5W–V, while 40W–V showed a slow consumption rate. We also confirmed N_2 production upon the introduction of $NO + O_2$, and a greater amount of N_2 was observed for 3.5W–V than for 0W–V (Fig. 6d, e, mass spectra), indicating that the production of N_2 was facilitated by the addition of tungsten. On the other hand, the MS intensity of N_2 was considerably low for 40W–V (Fig. 6f, mass spectra). These results suggested that NH_3-SCR activity decreases when an excess amount of tungsten is introduced to vanadium oxide because of high tungsten coverage that leads to blocking of the surface vanadium species as catalytically active sites despite the increase in acid sites.

To investigate the redox properties of the catalysts, we also conducted *operando* UV–Vis measurements (Fig. 7b and Supplementary Figs. 11 and 12). We monitored the change in the pseudo-absorbance (Kubelka–Munk unit) of UV–Vis spectra at $\lambda = 700$ nm (ΔKM_{700}), which is assigned to the *d–d* transition of V^{4+}, to observe the change in the valence of vanadium sites ($V^{5+} \leftrightarrow V^{4+}$). The production of N_2 was recorded simultaneously by an MS. The monitoring was performed under $NO + NH_3$ flowing followed by O_2 flowing to evaluate the respective reduction and oxidation half-cycles. The correlations between

W content, amount of V^{5+} reduced by $NO + NH_3$ (ΔKM_{700} under $NO + NH_3$ flowing), and MS intensity for N_2 are shown in Fig. 7b. The 3.5W–V showed the largest ΔKM_{700} and MS intensity of N_2 and had superior reduction capability for the production of N_2. On the other hand, ΔKM_{700} considerably decreased when 40 mol% of tungsten was doped, indicating that the catalyst with an excess amount of tungsten was difficult to be reduced. The 3.5W–V also showed the largest ΔKM_{700} under O_2 flowing (Supplementary Figs. 11b, d, f and 12b). Thus, 3.5W–V with moderate tungsten loading turned out to be the most redox-active catalyst, leading to the largest N_2 production. Combining with the results of *operando* IR measurements, tungsten sites serve as acid sites for the adsorption of ammonia, which is stronger than those pre-existing in vanadium oxide without tungsten, and the vanadium (V^{5+}) sites work as redox sites for NH_3-SCR. The highest activity for 3.5W–V can be ascribed to the increase in the number of acid sites and the high redox capability of the surface V species. W–O–V units would be needed for the progression of the reaction, and the number of adjacent tungsten sites such as W–O–W units becomes dominant with an increase in the amount of tungsten, leading to blocking of the surface redox-active V sites and thus resulting in a decrease in activity.

Effects of water on the NH_3-SCR cycle. The activity test clearly showed a positive effect of tungsten substitution in the presence of water. We also conducted *operando* IR measurements under a wet condition (2 vol% water) to check the effect of water on the acid sites for 0W–V and 3.5W–V. Although the IR peaks of adsorbed ammonia species on Lewis and Brønsted acid sites (NH_3 and NH_4^+, respectively) were both observed under a dry condition, the absorption band attributed to the NH_4^+ species was exclusively seen in the presence of water (Fig. 8a, b). The areas of the IR absorption band for Lewis and Brønsted acid sites under dry and wet conditions are shown in Fig. 8e, f. The area of

a

b
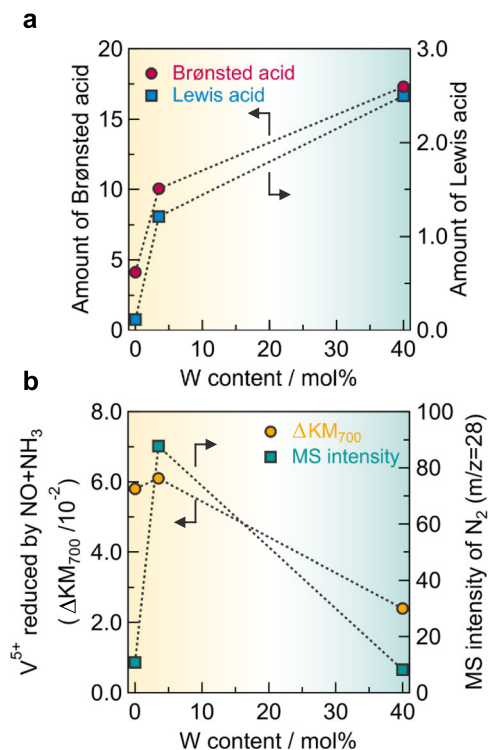
Fig. 7 Effect of tungsten on acid and redox properties. a Amount of Lewis and Brønsted acid sites as a function of W content. The amount of both acid sites was observed from the area of initial IR spectra after ammonia adsorption (spectra at 0 s in Fig. 6a–c). **b** Amount of V^{5+} reduced by $NO + NH_3$ and MS intensity of N_2 produced as a function of W content. The amount of V^{5+} reduced was determined from the change in the Kubelka–Munk unit at $\lambda = 700$ nm (ΔKM_{700}) under NO (500 ppm) + NH_3 (500 ppm) flowing (1500 s) at 150 °C under a dry atmosphere shown in Supplementary Figs. 7 and 8a.

the IR absorption band for NH_4^+ (Brønsted acid sites) increased from 10.0 (dry) to 18.7 (wet) and that for NH_3 (Lewis acid sites) decreased from 1.21 (dry) to 0.27 (wet) in the case of 3.5W–V when water vapor was introduced (3.5W–V; Fig. 8d–f). On the other hand, 0W–V showed only a slight change in the distribution of acid sites (0W–V; Fig. 8c, e, f). On a metal oxide surface, Lewis acid sites (coordinatively unsaturated metal cations) and Brønsted base sites (oxygen ions) can be changed into Brønsted acid sites by dissociative adsorption of water[58]. In a previous study, it was theoretically predicted that Brønsted acid sites (hydroxyl groups) are newly created on the V_2O_5–WO_3 solid solution by dissociative adsorption of water on tungsten-exposed sites and bridging oxygen sites under a wet atmosphere (Fig. 8g)[48]. On the other hand, water could be adsorbed on V_2O_5 without tungsten, but a Brønsted acid site does not form[47,48]. The observed changes in the surface state of vanadium oxide with and without tungsten can reflect such theoretical predictions. The area of the IR spectra (NH_4^+) decreased with time of $NO + O_2$ flowing both for 3.5W–V and 0W–V (Fig. 8c, d, red and blue lines), and ammonia species were consumed by the reaction under a wet condition. Considerable N_2 production was confirmed for 3.5W–V under a wet condition, but the N_2 production of 0W–V was smaller than that under a dry condition (Fig. 8c, d, mass spectra). These results suggest that NH_3-SCR of bulk vanadium oxide without tungsten is strongly inhibited by water, while bulk tungsten-substituted vanadium oxide proceeds with

the reaction by newly created protonic Brønsted acid sites that are less affected by water.

Operando UV–Vis measurements were also conducted for 3.5W–V with and without water vapor to check the redox cycle (Fig. 9 and Supplementary Fig. 13). NO (500 ppm) + NH_3 (500 ppm) and O_2 (8%) were repetitively introduced three times to confirm the redox cycle. During the measurements under wet and dry conditions, the pseudo-absorbance (KM unit) at $\lambda = 700$ nm similarly increased and decreased under $NO + NH_3$ and O_2 flowing, showing reduction ($V^{5+} \rightarrow V^{4+}$) and oxidation ($V^{4+} \rightarrow V^{5+}$) half-cycles (Fig. 9a–c for a wet condition and Supplementary Fig. 13 for a dry condition). The times of change in pseudo-absorbance (KM unit) at $\lambda = 700$ nm are shown by blue (wet) and red (dry) solid lines in Fig. 9d. Repetitive production of N_2 with a change in ΔKM_{700} was confirmed under both dry and wet atmospheres (Fig. 9d). Notably, considerable N_2 production was seen even in the presence of water (Fig. 9d, mass spectra). These results demonstrate that 3.5W–V proceeds with NH_3-SCR by the redox cycle and the N_2 production is not affected by water in a transient state.

Difference between supported and bulk vanadium oxide. *Operando* IR spectra were observed for 3.5W–V and V–W/TiO$_2$ to consider the difference between bulk and supported tungsten-substituted vanadium oxide catalysts. The measurement was conducted at 200 °C at which V–W/TiO$_2$ is sufficiently active and NO was flowed into samples after adsorption of NH_3 to obtain the information of acid sites next to redox sites (Supplementary Fig. 14). After the adsorption of NH_3 under a wet condition, NH_4^+ species adsorbed on Brønsted acid sites were solely confirmed for 3.5W–V (Fig. 10a), which was a similar result obtained at 150 °C in the presence of water. NH_4^+ species were rapidly consumed and significant N_2 production was confirmed when NO flowed (Fig. 10c). On the other hand, NH_3 species adsorbed on Lewis acid sites were mainly observed in addition to NH_4^+ species for V–W/TiO$_2$ (Fig. 10b). However, the consumption of NH_4^+ and NH_3 species were dull and N_2 production was less (Fig. 10c). The results demonstrate that Brønsted acid sites of 3.5W–V are more reactive than Brønsted and Lewis acid sites of V–W/TiO$_2$. After the above *operando* IR measurement under NO flowing for 3.5W–V, the sample was oxidized and NO flowed again to check if the residual NH_4^+ reacts with NO. Although the N_2 production and the consumption of NH_4^+ were attenuated under the first NO flowing (Fig. 10c), NH_4^+ species on Brønsted acid sites were consumed again and N_2 production was confirmed under the second NO flowing after oxidation (Supplementary Fig. 15). If *Operando* UV–Vis measurement was conducted in the same procedure ($NH_3 \rightarrow$ 1st $NO \rightarrow O_2 \rightarrow$ 2nd NO), the similar N_2 production behavior was observed accompanied by redox cycle ($V^{5+} \leftrightarrow V^{4+}$) under the first and second NO flowing (Supplementary Fig. 16). These results show that V sites reduced by the reaction of NH_4^+ (Brønsted acid site) with NO are re-oxidized, and remaining ammonia species move to Brønsted acid sites which are adjacent to redox V sites, then they react with NO by the re-oxidized V sites again. According to the previous reports on supported vanadium-based catalysts, Brønsted acid sites are not directly involved in the catalytic cycle and they play a role in an NH_3 pool to supply NH_3 to the Lewis acid sites[20,52]. In the case of bulk tungsten-substituted vanadium oxide catalyst, Brønsted acid site (B) would be located next to redox-active V^{5+} site and it would directly react with NO as following reduction half-cycle:

$$V(V) = O + NH_3(B) + NO \rightarrow V(IV) - OH + N_2 + H_2O.$$

$$(2)$$
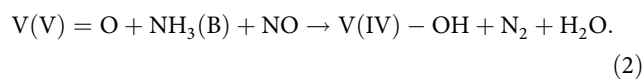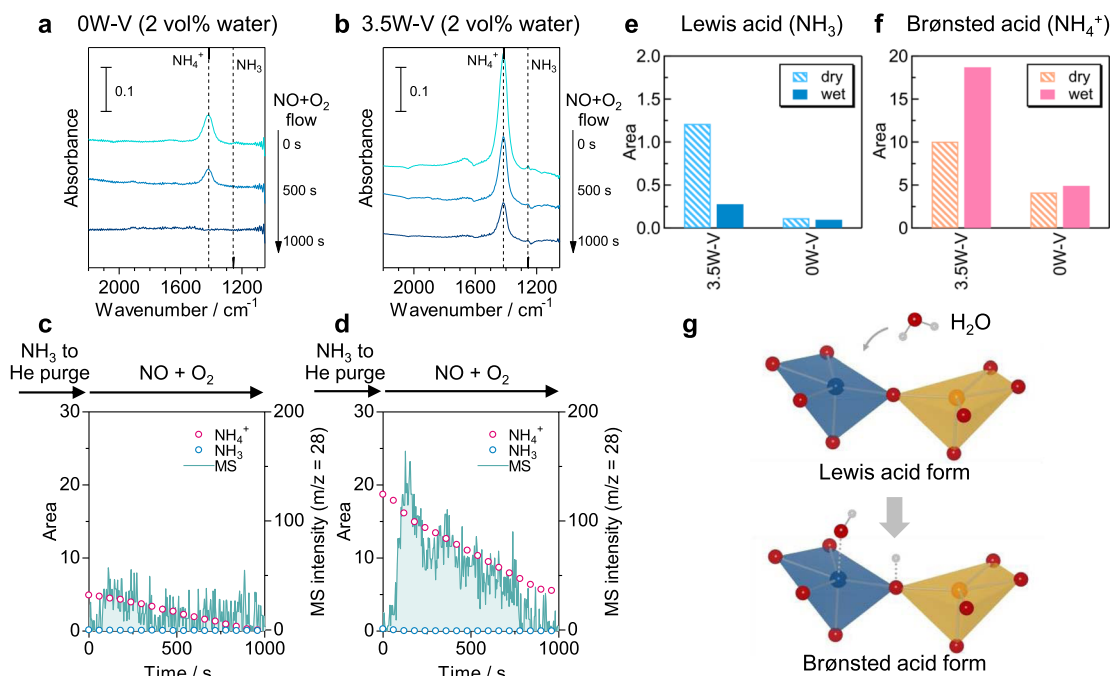
Fig. 8 Acid properties in the presence of water vapor. a, b *Operando* IR spectra of ad species on 0W–V (without tungsten) and 3.5W–V (with tungsten) during NH_3 adsorption, followed by $NO + O_2$ exposure at 150 °C under a wet condition (2 vol% water). The IR disc was exposed to 0.1% NH_3/He flow (30 min) and purged with He (20 min), followed by exposure to 500 ppm $NO + 8\% O_2 + 2\% H_2O$ (He balance) flow. **c, d** The IR peak areas of NH_3 adsorbed on Lewis acid sites (NH_3) and Brønsted acid sites (NH_4^+) and MS intensity of N_2 versus time of $NO + O_2$ flowing. IR areas for **e** Lewis acid and **f** Brønsted acid measured from IR spectra (0 s) under dry and wet conditions. **g** Metal-exposed surface of W-substituted vanadium oxide and its changes from Lewis acid form to Brønsted acid form. Orange polyhedra: vanadium units; blue polyhedra: tungsten units.

Furthermore, we conducted temperature-programmed reaction measurements under $NO + NH_3$ flow for 3.5W–V and V–W/TiO_2 (Supplementary Fig. 17) to observe the reducibility. The reduction of 3.5W–V started at ambient temperature, while a higher temperature was needed to reduce V–W/TiO_2. Bulk tungsten-substituted vanadium oxide catalyst has water-tolerant Brønsted acid sites and greater reducibility originated from bulk characteristics, resulting in high NH_3-SCR activity at a low temperature in the presence of water vapor.

Discussion

We investigated the low-temperature NH_3-SCR activity of tungsten-substituted vanadium oxide and the reaction mechanism under dry and wet conditions. The catalysts, 0–40 mol% tungsten-substituted vanadium oxide, were synthesized from ammonium metavanadate (NH_4VO_3) and ammonium metatungstate by the oxalate method. We confirmed from atomic-resolution HAADF-STEM images that the lattice vanadium sites were substituted by tungsten atoms, while adjacent and cluster tungsten moieties were found when an excess amount of tungsten was doped up to 40 mol%. XRD measurements also showed that the WO_3 phase was generated in catalysts with an increase in the molar ratio of >3.5 mol%. The 3.5W–V catalyst showed the highest NO conversions, >99% (dry) and ~93% (wet, 10 vol% water). The NO conversion decreased when >3.5 mol% of tungsten was added to vanadium oxide. The stability of the catalysts was increased by the addition of tungsten because bulk WO_6 units connected vanadium oxide layers. The reaction mechanism was investigated for 0W–V (V_2O_5 without tungsten), 3.5W–V (the best active catalyst), and 40W–V (excess tungsten) using *operando* IR and UV–Vis measurements. It was found that the vanadium site plays a role as a redox site and the tungsten site

contributed to the acid sites for adsorption of ammonia. With an increase in tungsten, the activity decreased because the number of redox sites decreased for high tungsten coverage despite the increase in the number of acid sites. Acid sites of tungsten-substituted vanadium oxide were converted to Brønsted acid sites under a wet condition, while vanadium oxide without tungsten did not show a significant change in the population. From *operando* UV–Vis measurements, 3.5 mol% tungsten-substituted vanadium oxide showed high redox capabilities even in the presence of water, and N_2 production during the reduction half-cycle was hardly affected by the addition of water. The 3.5W–V catalyst had the high redox ability and reactivity of Brønsted acid sites at a low temperature in the presence of water. These results evidence water tolerance of bulk tungsten-substituted vanadium oxide. Although our results experimentally demonstrated the effect of water on the NH_3-SCR cycle over the V–W oxide system, the detailed reaction mechanism needs to be elucidated since water molecules may participate in each elementary reaction step. The acid and redox properties and the effect of water would also change depending on various factors such as the morphology, exposed facet, and surface reconstruction. We believe that our results provide a better understanding of NH_3-SCR at a low temperature, which is a future task for the current deNOx process.

Methods

Synthesis of tungsten-substituted vanadium oxide catalysts. First, NH_4VO_3 and oxalic acid (11.9 g, 131.7 mmol) were dissolved in 50 mL of water and the aqueous solution was stirred for 10 min for completion of the change in color of
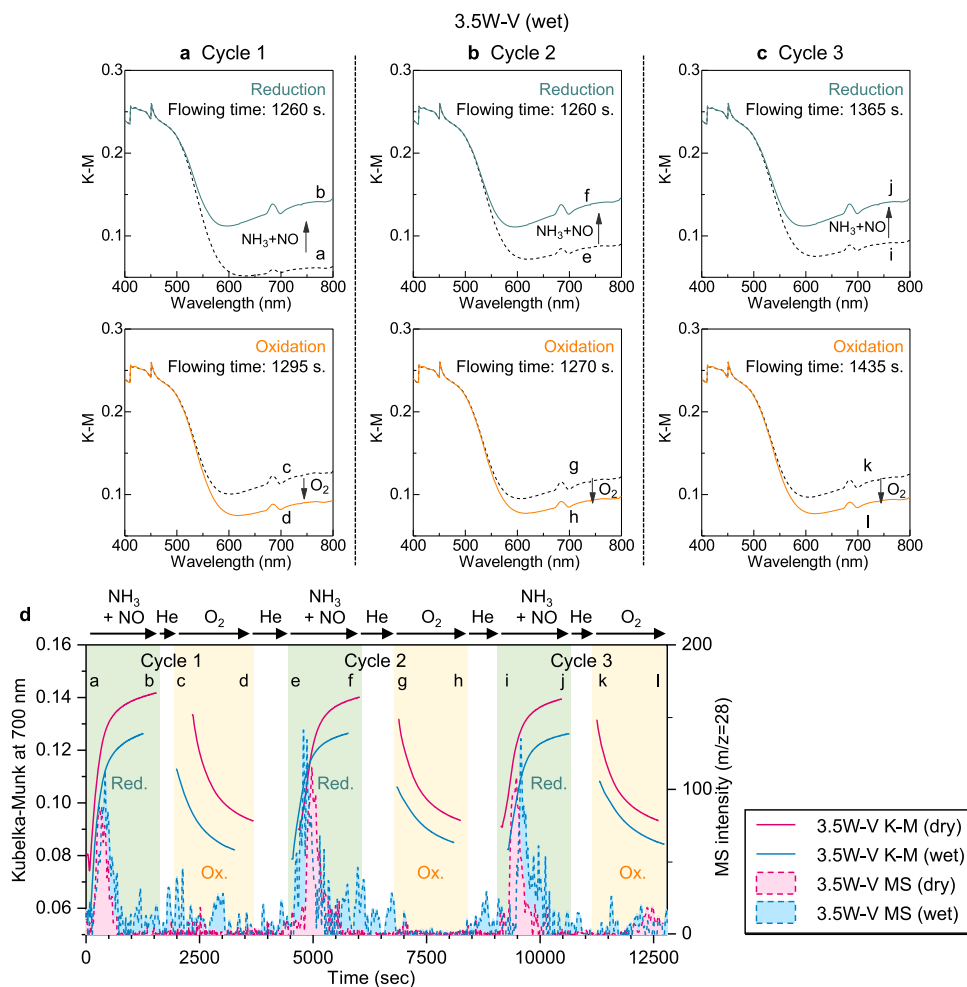
Fig. 9 Redox properties of W-substituted vanadium oxide (3.5W–V) under wet and dry conditions. *Operando* UV–Vis spectra of 3.5W–V for reduction (500 ppm NO + 500 ppm NH$_3$) and oxidation (8% O$_2$) half-cycles at 150 °C under a wet (2 vol% water) atmosphere for the **a** first cycle, **b** second cycle, and **c** third cycle. **d** Change in the Kubelka–Munk unit at $\lambda = 700$ nm and MS intensity of N$_2$ as a function of time for 3.5W–V during NO (500 ppm) + NH$_3$ (500 ppm) and O$_2$ (8%) flowing at 150 °C under a dry atmosphere and wet (2 vol% water) atmosphere. The characters a–l correspond to the points at which the UV–Vis spectra were observed.
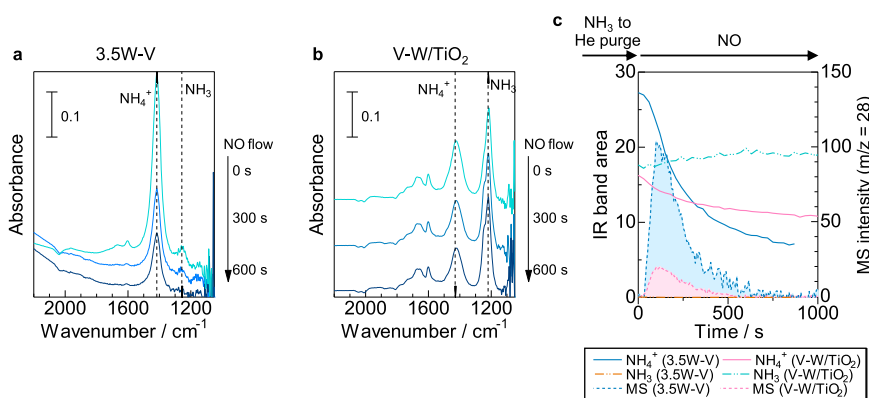
Fig. 10 Difference between bulk and supported catalysts. *Operando* IR spectra of ad species on **a** 3.5W–V (bulk W-substituted vanadium oxide) and **b** V–W/TiO$_2$ (supported catalyst) during NH$_3$ adsorption in the presence of water followed by NO exposure at 200 °C. The IR disc was exposed to 0.1% NH$_3$/He flow in the presence of 2% water vapor (30 min) and purged with He (20 min), followed by exposure to 500 p.pm NO (He balance) flow. **c** IR peak areas of ammonia species adsorbed on Brønsted acid sites (NH$_4$+) and MS intensity of N$_2$ versus time of NO flowing.

the solution. Next, ammonium metatungstate was added to the solution. Then, the solution was heated overnight to evaporate the water on a hotplate. Finally, the resulting solid was calcined twice at 300 °C for 4 h each time. The sample was denoted as xW–V, where x is the molar ratio (mol%) of W to V. The amounts of reagents are shown in Supplementary Table 1.

Synthesis of TiO$_2$-supported V$_2$O$_5$/WO$_3$ (1 wt% V$_2$O$_5$–5 wt% WO$_3$/TiO$_2$).
First, vanadium and tungsten precursor aqueous solutions were prepared. For the vanadium precursor aqueous solution, 0.020 g of NH$_4$VO$_3$ (0.17 mmol) and 0.045 g of oxalic acid (0.51 mmol) were dissolved in 2 mL of water and the aqueous solution was stirred for 10 min. For the tungsten precursor aqueous solution, 0.084

g of ammonium metatungstate hydrate (0.028 mmol) and 0.089 g of oxalic acid (0.99 mmol) were dissolved in 2 mL of water and the aqueous solution was stirred for 10 min. Then. 1.4 g of TiO_2 (P25) was added to 20 mL water and the vanadium and tungsten precursor aqueous solutions were added to the dispersion. The dispersion was then heated at 120 °C to evaporate the water. Finally, the resulting solid was calcined at 300 °C for 4 h.

Catalyst characterization. STEM images were obtained by using FEI Titan Cubed G2 60–300. For TEM measurements, samples were deposited on a carbon film-coated mesh copper grid. XRD patterns were collected by SmartLab (Rigaku) with Cu Kα radiation. Rietveld analyses were carried out using Reflex program in Materials Studio 2017.

Catalytic activity test. The NH_3-SCR activity of vanadium oxide catalysts was measured using a fixed-bed flow reactor (Supplementary Fig. 1). The reaction gas mixture, 250 ppm NO, 250 ppm NH_3, 4 vol% O_2 and 5–20 vol% water (when used) in Ar (250 mL min^{-1}), was fed to the catalyst (0.375 g). The outlet gases were analyzed by an IR spectrometer (JASCO FT/IR-4700) equipped with a gas cell (JASCO LPC12M-S). NO conversion and N_2 selectivity were calculated by the following equations:

$$NO\ conversion(\%) = \frac{NO_{in} - NO_{out}}{NO_{in}} \times 100, \tag{3}$$

$$N_2\ selectivity(\%)\ \frac{2 \times N_{2out}}{(NO_{in} + NH_{3in}) - (NO_{out} + NH_{3out})}$$
$$(2 \times N_{2out} = (NO_{in} + NH_{3in}) - (NO_{out} + NH_{3out} + NO_{2out} + 2 \times N_2O_{out})). \tag{4}$$

Reaction rate and reaction order of the catalysts were determined by adjusting the amount of catalysts and the flow rate for NO conversion to be below 20%.

Operando FT-IR measurements. *Operando* FT-IR spectra were recorded at 150 °C using a JASCO FT/IR-4200 with a TGS (triglycine sulfate) detector. Samples (each 40 mg) were pressed to obtain self-supporting pellets ($\phi = 20$ mm), which were placed in a quartz IR cell with CaF_2 windows connected to a conventional gas flow system. Prior to measurements, the sample pellets were heated under a flow of 10% O_2/He (100 mL min^{-1}) at 300 °C for 10 min. NH_3/He (0.1%) was then introduced for 0.5 h, and subsequently, the gas was switched to He (20 min) in order to let the residual NH_3 gas out. After taking the first spectrum, 500 ppm NO, 8% O_2 (when used)/He was introduced to the sample at a flow rate of 100 mL min^{-1}. For the measurement under a wet condition, 2% H_2O was introduced. Spectra were measured by accumulating 20 scans at a resolution of 4 cm^{-1}. A reference spectrum taken at 150 °C under He flow was subtracted from each spectrum. An MS (BELMass, MicrotracBEL Corp.) was used for the analysis of N_2 gas.

Operando UV-Vis measurements. Diffuse reflectance UV–Vis measurements were conducted at 150 °C with a UV–Vis spectrometer (JASCO V-670) connected to an *operando* flow cell with a quartz window. The light source was led to an integrating sphere through an optical fiber. Samples (each 10 mg) were placed in the sample cell connected to a gas flow system. Reflectance was converted to KM units using the KM function. A background spectrum was corrected by measuring $BaSO_4$. Prior to measurements, the sample pellets were heated under a flow of 10% O_2/He (100 mL min^{-1}) at 300 °C for 10 min. Then, the sample pellets were cooled down to 150 °C. The measurements were performed by the following steps: (i) The sample pellets were purged with He flow to remove residual oxygen and the initial UV–Vis spectra were measured (spectra 1). (ii) A gas mixture (500 ppm NH_3 + 500 ppm NO/He) was fed to a sample at a flow rate of 100 mL min^{-1} for a given time. Then, UV–vis spectra were recorded (spectra 2). (iii) After turning off the gas flow, the sample pellets were purged with He flow followed by UV–Vis spectra acquisition (spectra 3). (iv) Then, a gas mixture (8% O_2/He) was fed to a sample at a flow rate of 100 mL min^{-1} for a given time and UV–Vis spectra were obtained (spectra 4). Steps (i)–(iv) were regarded as one cycle. The change in the KM unit at $\lambda = 700$ nm (ΔKM_{700}), which was assigned to the d–d transition of V^{4+}, was measured to obtain the relative amount of redox sites. ΔKM_{700} values for reduction (V^{5+} reduced by $NO + NH_3$) and oxidation (V^{4+} oxidized by O_2) half-cycles were calculated by the following equations:

$$(\Delta KM_{700}\ for\ reduction\ half\ cycle) = (KM_{700}\ in\ spectra\ 2) - (KM_{700}\ in\ spectra\ 1), \tag{5}$$

$$(\Delta KM_{700}\ for\ oxidation\ half\ cycle) = (KM_{700}\ in\ spectra\ 4) - (KM_{700}\ in\ spectra\ 3). \tag{6}$$

The production of N_2 in the outlet gas mixture was monitored by an MS (BELMass, MicrotracBEL Corp.).

Others. The crystal structure was drawn by VESTA[59].

References

1. Han, L. et al. Selective catalytic reduction of NOx with NH_3 by using novel catalysts: state of the art and future prospects. *Chem. Rev.* **119**, 10916–10976 (2019).
2. Lai, J. & Wachs, I. E. A perspective on the selective catalytic reduction (SCR) of NO with NH_3 by supported V_2O_5-WO_3/TiO_2 catalysts. *ACS Catal.* **8**, 6537–6551 (2018).
3. Marberger, A., Elsener, M., Ferri, D. & Kröcher, O. VOx surface coverage optimization of V_2O_5/WO_3-TiO_2 SCR catalysts by variation of the V loading and by aging. *Catalysts* **5**, 1704–1720 (2015).
4. Nakajima, F. & Hamada, I. The state-of-the-art technology of NOx control. *Catal. Today* **29**, 109–115 (1996).
5. Boningari, T. & Smirniotis, P. G. Impact of nitrogen oxides on the environment and human health: Mn-based materials for the NOx abatement. *Curr. Opin. Chem. Eng.* **13**, 133–141 (2016).
6. Peng, Y., Chang, H., Dai, Y. & Li, J. Structural and Surface Effect of MnO_2 for Low Temperature Selective Catalytic Reduction of NO with NH_3. *Procedia Environ. Sci.* **18**, 384–390 (2013).
7. Smirniotis, P. G., Peña, D. A. & Uphade, B. S. Low-Temperature Selective Catalytic Reduction (SCR) of NO with NH_3 by Using Mn, Cr, and Cu Oxides Supported on Hombikat TiO_2. *Angew. Chem. Int. Ed.* **40**, 2479–2482 (2001).
8. Xu, H. et al. Design and synthesis of highly-dispersed WO_3 catalyst with highly effective NH_3-SCR activity for NOx abatement. *ACS Catal.* **9**, 11557–11562 (2019).
9. Gillot, S. et al. Development of stable and efficient $CeVO_4$ systems for the selective reduction of NOx by ammonia: structure-activity relationship. *Appl. Catal. B* **218**, 338–348 (2017).
10. Huang, L. et al. Hydrothermal growth and characterization of length tunable porous iron vanadate one-dimensional nanostructures. *CrystEngComm* **16**, 5128–5133 (2014).
11. Nakasaka, Y. et al. Micropore diffusivities of NO and NH_3 in Cu-ZSM-5 and their effect on NH_3-SCR. *Catal. Today* **332**, 64–68 (2019).
12. Sullivan, J. A. & Keane, O. The role of Bronstead acidity in poisoning the SCR-urea reaction over FeZSM-5 catalysts. *Appl. Catal. B* **61**, 244–252 (2005).
13. Kieffer, C., Lavy, J., Jeudy, E., Bats, N. & Delahay, G. Characterisation of a commercial automotive NH_3-SCR copper-zeolite catalyst. *Top. Catal.* **56**, 40–44 (2013).
14. De-La-Torre, U., Pereda-Ayo, B., Moliner, M., González-Velasco, J. R. & Corma, A. Cu-zeolite catalysts for NO_x removal by selective catalytic reduction with NH_3 and coupled to NO storage/reduction monolith in diesel engine exhaust aftertreatment systems. *Appl. Catal. B* **187**, 419–427 (2016).
15. Fahami, A. R. et al. The dynamic nature of Cu sites in Cu-SSZ-13 and the origin of the seagull NO_x conversion profile during NH_3-SCR. *React. Chem. Eng.* **4**, 1000–1018 (2019).
16. Song, J. et al. Toward rational design of Cu/SSZ-13 selective catalytic reduction catalysts: implications from atomic-level understanding of hydrothermal stability. *ACS Catal.* **7**, 8214–8227 (2017).
17. Kwak, J. H., Tonkyn, R. G., Kim, D. H., Szanyi, J. & Peden, C. H. F. Excellent activity and selectivity of Cu-SSZ-13 in the selective catalytic reduction of NO_x with NH_3. *J. Catal.* **275**, 187–190 (2010).
18. Inomata, Y. et al. Bulk vanadium oxide versus conventional V_2O_5/TiO_2: NH_3-SCR catalysts working at a low temperature below 150 °C. *ACS Catal.* **9**, 9327–9331 (2019).
19. Inomata, Y. et al. Synthesis of bulk vanadium oxide with a large surface area using organic acids and its low-temperature NH_3-SCR activity. *Catal. Today* https://doi.org/10.1016/j.cattod.2020.06.041 (2020).
20. He, G. et al. Polymeric vanadyl species determine the low-temperature activity of V-based catalysts for the SCR of NO_x with NH_3. *Sci. Adv.* **4**, eaau4637 (2018).
21. Qu, W. et al. Single-atom catalysts reveal the dinuclear characteristic of active sites in NO selective reduction with NH_3. *Nat. Commun.* **11**, 1–7 (2020).
22. Ganjkhanlou, Y. et al. Location and activity of VOx species on TiO_2 particles for NH_3-SCR catalysis. *Appl. Catal. B* **278**, 119337 (2020).
23. Wachs, I. E. Catalysis science of supported vanadium oxide catalysts. *Dalton Trans.* **42**, 11762–11769 (2013).
24. Kristoffersen, H. H. & Metiu, H. Reconstruction of low-index α-V_2O_5 surfaces. *J. Phys. Chem. C* **119**, 10500–10506 (2015).

25. Wachs, I. E. The generality of surface vanadium oxide phases in mixed oxide catalysts. *Appl. Catal. A* **391**, 36–42 (2011).

26. Wang, Q. et al. Research progress on vanadium-based cathode materials for sodium ion batteries. *J. Mater. Chem. A* **6**, 8815–8838 (2018).

27. Bahlawane, N. & Lenoble, D. Vanadium oxide compounds: structure, properties, and growth from the gas phase. *Chem. Vap. Depos.* **20**, 299–311 (2014).

28. Weckhuysen, B. M. & Keller, D. E. Chemistry, spectroscopy and the role of supported vanadium oxides in heterogeneous catalysis. *Catal. Today* **78**, 25–46 (2003).

29. Wang, Y., Takahashi, K., Shang, H. & Cao, G. Synthesis and electrochemical properties of vanadium pentoxide nanotube arrays. *J. Phys. Chem. B* **109**, 3085–3088 (2005).

30. Wei, Y., Ryu, C. W. & Kim, K. B. Cu-doped V_2O_5 as a high-energy density cathode material for rechargeable lithium batteries. *J. Alloy. Compd.* **459**, L13–L17 (2008).

31. Grégoire, G., Baffier, N., Kahn-Harari, A. & Badot, J. C. X-ray powder diffraction study of a new vanadium oxide $Cr_{0.11}V_2O_{5.16}$ synthesized by a sol-gel process. *J. Mater. Chem.* **8**, 2103–2108 (1998).

32. Jovanović, A. et al. Structural and electronic properties of V_2O_5 and their tuning by doping with 3d elements-modelling using the DFT+ U method and dispersion correction. *Phys. Chem. Chem. Phys.* **20**, 13934–13943 (2018).

33. Kaper, H. et al. Ionic liquid- and surfactant-controlled crystallization of WO_3 films. *Phys. Chem. Chem. Phys.* **17**, 18138–18145 (2015).

34. Mardare, C. C. & Hassel, A. W. Review on the versatility of tungsten oxide coatings. *Phys. Stat. Sol.* **216**, 1900047 (2019).

35. Wang, S., Fan, W., Liu, Z., Yu, A. & Jiang, X. Advances on tungsten oxide based photochromic materials: strategies to improve their photochromic properties. *J. Mater. Chem. C* **6**, 191–212 (2018).

36. Jaegers, N. R. et al. Mechanism by which tungsten oxide promotes the activity of supported V_2O_5/TiO_2 catalysts for NO_X abatement: structural effects revealed by ^{51}V MAS NMR spectroscopy. *Angew. Chem. Int. Ed.* **58**, 12609–12616 (2019).

37. Lintz, H. G. & Turek, T. Intrinsic kinetics of nitric oxide reduction by ammonia on a vanadia-titania catalyst. *Appl. Catal. A* **85**, 13–25 (1992).

38. Dumesic, J. A., Topsøe, N. Y., Topsøe, H., Chen, Y. & Slabiak, T. Kinetics of selective catalytic reduction of nitric oxide by ammonia over vanadia/titania. *J. Catal.* **163**, 409–417 (1996).

39. Lietti, L., Nova, I. & Forzatti, P. Selective catalytic reduction (SCR) of NO by NH_3 over TiO_2-supported V_2O_5-WO_3, V_2O_5-MoO_3 catalysts. *Top. Catal.* **11–12**, 111–122 (2000).

40. Turco, M., Lisi, L., Pirone, R. & Ciambelli, P. Effect of water on the kinetics of nitric oxide reduction over a high-surface-area V_2O_5/TiO_2 catalyst. *Appl. Catal. B* **3**, 133–149 (1994).

41. Tufano, V. & Turco, M. Kinetic modelling of nitric oxide reduction over a high-surface area V_2O_5-TiO_2 catalyst. *Appl. Catal. B* **2**, 9–26 (1993).

42. Long, R. Q. & Yang, R. T. Selective catalytic reduction of NO with ammonia over V_2O_5 doped TiO_2 pillared clay catalysts. *Appl. Catal. B* **24**, 13–21 (2000).

43. Forzatti, P. Present status and perspectives in de-NOx SCR catalysis. *Appl. Catal. A* **222**, 221–236 (2001).

44. Forzatti, P. Environmental catalysis for stationary applications. *Catal. Today* **62**, 51–65 (2000).

45. Topsøe, N.-Y., Slabiak, T., Clausen, B. S., Srnak, T. Z. & Dumesic, J. A. Influence of water on the reactivity of vanadia/titania for catalytic reduction of NOx. *J. Catal.* **134**, 742–746 (1992).

46. Nova, I., Lietti, L., Tronconi, E. & Forzatti, P. Transient responce method applied to the kinetic analysis of the DeNOx-SCR reaction. *Chem. Eng. Sci.* **56**, 1229–1237 (2001).

47. Yin, X. et al. Adsorption of H_2O on the V_2O_5 (010) surface studied by periodic density functional calculations. *J. Phys. Chem. B* **103**, 3218–3224 (2002).

48. Broclawik, E., Góra, A. & Najbar, M. The role of tungsten in formation of active sites for no SCR on the V-W-O catalyst surface—quantum chemical modeling (DFT). *J. Mol. Catal. A* **166**, 31–38 (2001).

49. Da Costa, A. et al. Observation of the V_2O_5(001) surface using ambient atomic force microscopy. *Surf. Sci.* **370**, 339–344 (1997).

50. Inomata, M., Miyamoto, A. & Murakami, Y. Mechanism of the reaction of NO and NH_3 on vanadium oxide catalyst in the presence of oxygen under the dilute gas condition. *J. Catal.* **62**, 140–148 (1980).

51. Zhu, M., Lai, J.-K., Tumuluri, U., Wu, Z. & Wachs, I. E. Nature of active sites and surface intermediates during SCR of NO with NH_3 by supported V_2O_5–WO_3/TiO_2 catalysts. *J. Am. Chem. Soc.* **139**, 15624–15627 (2017).

52. Marberger, A., Ferri, D., Elsener, M. & Kröcher, O. The significance of Lewis acid sites for the selective catalytic reduction of nitric oxide on vanadium-based catalysts. *Angew. Chem.* **55**, 11989–11994 (2016).

53. Topsøe, N. Y., Dumesic, J. A. & Topsøe, H. Vanadia-titania catalysts for selective catalytic reduction of nitric-oxide by ammonia. II. Studies of active sites and formulation of catalytic cycles. *J. Catal.* **151**, 241–252 (1995).

54. Topsøe, N. Y., Topsøe, H. & Dumesic, J. A. Vanadia/titania catalysts for selective catalytic reduction (SCR) of nitric-oxide by ammonia. I. Combined temperature-programmed in-situ ftir and on-line mass-spectroscopy studies. *J. Catal.* **151**, 226–240 (1995).

55. Song, I., Lee, H., Jeon, S. W. & Kim, D. H. Understanding the dynamic behavior of acid sites on TiO_2-supported vanadia catalysts via operando DRIFTS under SCR-relevant conditions. *J. Catal.* **382**, 269–279 (2020).

56. Satsuma, A. et al. Surface active sites of vanadium pentoxide-tungsten trioxide catalysts. *J. Phys. Chem.* **92**, 6052–6058 (1988).

57. Busca, G., Lietti, L., Ramis, G. & Berti, F. Chemical and mechanistic aspects of the selective catalytic reduction of NO(x) by ammonia over oxide catalysts: a review. *Appl. Catal. B* **18**, 1–36 (1998).

58. Kung, H. H. *Transition Metal Oxides: Surface Chemistry and Catalysis* (Elsevier, 1989).

59. Momma, K. & Izumi, F. VESTA 3 for three-dimensional visualization of crystal, volumetric and morphology data. *J. Appl. Crystallogr.* **44**, 1272–1276 (2011).

Acknowledgements

Author contributions
Y.I. and T.M. conceived the original concept and designed the experiments. Y.I. conducted the experiments and wrote the manuscript. H.K. carried out the operando UV measurements and helped Y.I. to measure operando IR spectra. T.T. and K.-i.S. supervised the operando measurements and supported the analysis of the results. S.I. and W.U. conducted the Rietveld analysis. S.H. helped synthesis catalysts. N.S. carried out HAADF-STEM measurements. E.K., K.M., and K.Y. supported catalytic activity test. M.H. gave advice about the interpretation of the results. T.M. supervised this project. All authors contributed to discuss the results.

Competing interests
The authors declare no competing interests.

Additional information
Supplementary information is available for this paper at https://doi.org/10.1038/s41467-020-20867-w.

Correspondence and requests for materials should be addressed to T.M.

Peer review information *Nature Communications* thanks Gloria Berlier, JianZhi Hu and Hong He for their contribution to the peer review of this work. Peer reviewer reports are available.

Reprints and permission information is available at http://www.nature.com/reprints

Publisher's note Springer Nature remains neutral with regard to jurisdictional claims in published maps and institutional affiliations.